Supplemental Material can be found at:
http://www.jbc.org/content/suppl/2011/06/21/M111.250944.DC1.html

THE JOURNAL OF BIOLOGICAL CHEMISTRY VOL. 286, NO. 33, pp. 29146–29157, August 19, 2011
© 2011 by The American Society for Biochemistry and Molecular Biology, Inc. Printed in the U.S.A.

Pyrovanadolysis, a Pyrophosphorolysis-like Reaction Mediated by Pyrovanadate, Mn^{2+}, and DNA Polymerase of Bacteriophage T7*[S]

Received for publication, April 13, 2011, and in revised form, May 23, 2011 Published, JBC Papers in Press, June 21, 2011, DOI 10.1074/jbc.M111.250944

Barak Akabayov[‡], Arkadiusz W. Kulczyk[‡], Sabine R. Akabayov[‡], Christopher Theile[‡], Larry W. McLaughlin[§], Benjamin Beauchamp[‡], Antoine M. van Oijen[¶], and Charles C. Richardson[‡1]

From the [‡]Department of Biological Chemistry and Molecular Pharmacology, Harvard Medical School, Boston, Massachusetts 02115, the [§]Department of Chemistry, Merkert Chemistry Center, Boston College, Chestnut Hill, Massachusetts 02467, and [¶]Zernike Institute for Advanced Materials Centre for Synthetic Biology, Nijenborgh 4, 9747 AG Groningen, The Netherlands

DNA polymerases catalyze the 3′–5′-pyrophosphorolysis of a DNA primer annealed to a DNA template in the presence of pyrophosphate (PP_i). In this reversal of the polymerization reaction, deoxynucleotides in DNA are converted to deoxynucleoside 5′-triphosphates. Based on the charge, size, and geometry of the oxygen connecting the two phosphorus atoms of PP_i, a variety of compounds was examined for their ability to carry out a reaction similar to pyrophosphorolysis. We describe a manganese-mediated pyrophosphorolysis-like activity using pyrovanadate (VV) catalyzed by the DNA polymerase of bacteriophage T7. We designate this reaction pyrovanadolysis. X-ray absorption spectroscopy reveals a shorter Mn-V distance of the polymerase-VV complex than the Mn-P distance of the polymerase-PP_i complex. This structural arrangement at the active site accounts for the enzymatic activation by Mn-VV. We propose that the Mn^{2+}, larger than Mg^{2+}, fits the polymerase active site to mediate binding of VV into the active site of the polymerase. Our results may be the first documentation that vanadium can substitute for phosphorus in biological processes.

Gene 5 of bacteriophage T7 encodes a DNA polymerase essential for replication of the T7 genome (1). T7 DNA polymerase forms a complex with *Escherichia coli* thioredoxin (trx),[2] an interaction that increases its processivity of nucleotide polymerization several hundredfold (2). The structure of T7 DNA polymerase in complex with trx is shown in Fig. 1. The structure closely resembles that of *E. coli* DNA polymerase I, thus placing it in the polymerase I family of DNA polymerases (3). In this study, we designate the polymerase in complex with trx as T7 DNA polymerase. Like most other prokaryotic DNA polymerases, T7 DNA polymerase has a proofreading 3′–5′-exonuclease activity located in the amino-terminal half of the protein (3). The crystal structure shows that its active site is located between the "fingers" and the "palm" subdomains and contains two magnesium ions (Mg^{2+}). During polymerization of nucleotides, the Mg^{2+} closest to the primer (catalytic Mg^{2+}) is responsible for deprotonation of the 3′-hydroxyl group of the primer prior to its nucleophilic attack on the α-phosphate of the incoming dNTP. The second Mg^{2+} (structural Mg^{2+}) is associated with stabilization of the reactive state of the β- and γ-phosphates of the incoming deoxynucleoside 5′-triphosphate (dNTP) (4).

In the presence of PP_i, DNA polymerases catalyze the 3′–5′-degradation of a DNA primer annealed to a DNA template (5). In this reaction, known as pyrophosphorolysis, the deoxynucleotides (dNMP) of the DNA are converted to dNTP. Pyrophosphorolysis is a true reversal of the polymerization reaction in that the products are dNTPs, and it has the same requirements for a template and a 3′-hydroxyl-terminated primer (5). The 3′–5′-exonuclease associated with DNA polymerase, however, catalyzes the 3′–5′ hydrolysis of the primer to yield dNMPs without a strict requirement for proper base pairing. Pyrophosphorolysis occurs in the polymerase active site, unlike the exonuclease activity that occurs in a separate domain of the protein containing the exonuclease active site (3).

The pyrophosphate released during DNA synthesis *in vivo* is hydrolyzed to inorganic orthophosphate by the abundant pyrophosphatase present in cells, essentially leading to an irreversible reaction (6). However, inhibition of pyrophosphatase or transient localization of pyrophosphate near the active site can result in pyrophosphorolysis. Such a reversal in the reaction would enable polymerases such as the Y family of DNA polymerases or RNA polymerases lacking a proofreading exonuclease activity to use pyrophosphorolysis as an alternative means of proofreading (7). Pyrophosphorolysis can create problems during DNA sequence analysis using DNA polymerases because pyrophosphate accumulates during the reaction (8).

E. coli DNA polymerase I catalyzes an exchange reaction between pyrophosphate and dNTPs (5). The exchange reaction has strict base specificity for activation and a requirement for both a template strand and a 3′-hydroxyl-terminated primer

* This work was supported, in whole or in part, by National Institutes of Health Grant GM54397 (to C. C. R.) and by Center for Synchrotron Biosciences Grant P30-EB-009998 from the National Institute of Biomedical Imaging and Bioengineering. This work was supported by Grant from the National Science Foundation (to L. W. M.).

[S] The on-line version of this article (available at http://www.jbc.org) contains supplemental Figs. S1–S5, Table S1, and additional references.

[1] To whom correspondence should be addressed: Dept. of Biological Chemistry and Molecular Pharmacology, Harvard Medical School, 240 Longwood Ave., Boston, MA 02115. Tel.: 617-432-1864; Fax: 617-432-3362; E-mail: ccr@hms.harvard.edu.

[2] The abbreviations used are: trx, thioredoxin; PDB, Protein Data Bank; VV, pyrovanadate; XAFS, x-ray absorption fine structure; dNPVV, deoxyribonucleoside monophosphate divanadate; EXAFS, extended XAFS.

Downloaded from www.jbc.org at HARVARD UNIVERSITY, on August 13, 2011

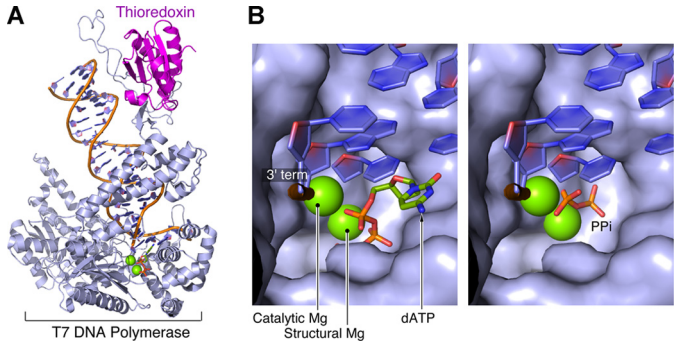

FIGURE 1. **Crystal structure of the active site of phage T7 DNA polymerase (PDB entry 1T8E).** *A,* T7 DNA polymerase in complex with thioredoxin, a primer-template, and a dNTP in the active site. The two Mg^{2+} ions are shown in *green*. *B,* enlargement of the active site of T7 DNA polymerase containing the 3′ terminus of the primer with the two Mg^{2+} ions (*green*) and dATP (*left*) or PP_i (*right*) from an overlay of the two metal ions in the Dpo4 crystal structure together with PP_i (PDB entry 2ago). The structural alignment and figure preparation were created using PyMOL. The two Mg^{2+} ions are coordinated through the protein side chain moieties and the phosphate backbone of the DNA and NTP or PP_i.

(5). These properties indicate that PP_i exchange occurs when the formation of a diester bond is followed by an attack of PP_i on the newly incorporated dNTP at the 3′-end of the primer.

In studies on polymerase function, pyrophosphate analogues such as phosphonoformic acid and phosphonoacetic acid have been used to inhibit DNA polymerase activity (9). Methylene bis(arsenic acid), arsonomethylphosphonic acid, and arsonoacetic acid can replace PP_i in a pyrophosphorolysis-like reaction (10). In these cases, the product of the arsenic complex-mediated pyrophosphorolysis-like reaction is deoxynucleoside 5′-monophosphate (dNMP). The ability of molecules such as arsenate to substitute for naturally occurring molecules *in vitro* is well documented. It has been reported recently that a strain of Halomonadaceae can even substitute arsenate for phosphate for growth (11). Such bacteria with DNA containing arsenate instead of phosphate backbone would have to invest extensive effort to protect the DNA from hydrolysis because of low kinetic stability in aqueous solution (12). In any case, molecules with a molecular structure similar to PP_i are candidates for inhibiting polymerase or for mediating a pyrophosphorolysis-like reaction. In this context, pyrovanadate is a natural candidate. Vanadate is structurally and electronically similar to phosphate and serves as a potent inhibitor for a variety of phosphate-binding enzymes (13). However, there are also significant chemical differences between vanadate and phosphate. The atomic radius of vanadium is larger than the atomic radius of phosphorus, 1.34 and 0.93 Å, respectively, resulting in longer V–O bonds relative to P–O bonds. The geometry of vanadate and the partially occupied *d*-orbital of vanadium result in a 6–7-fold greater thermodynamic stability of vanadate anhydrides in comparison with that of phosphate anhydrides (13, 14).

Pyrovanadate (VV) is a dimeric form of vanadate and as such has the potential to bind specifically to the active site of enzymes that would normally bind PP_i. Although the formation of phosphovanadate anhydride has been described (9, 15), most studies have only examined the effect of the monomeric vanadate on biological processes. The chemical formation of phosphovanadyl has been studied previously (16) but not in a biological context. Binding of VV to phosphoglycerate mutase was found to activate the enzyme and the transfer of phosphate directly to a water molecule (17). A crystal structure of VV bound in the active site of the tyrosine phosphatase YopH has been reported recently (18). To our knowledge, these examples are among the few structural and biochemical evidences for the binding and activation of an enzymatic reaction by VV.

In this study, we show that T7 DNA polymerase in the presence of Mn^{2+} ions catalyzes a pyrophosphorolysis-like reaction using VV as a substrate. We have used x-ray absorption fine structure (XAFS) to address the structural basis for this phenomenon. Thus far, structural studies of the active sites of DNA polymerases have, for the most part, been limited to x-ray crystallography. X-ray absorption spectroscopy allows detection of changes in the metal sites of metalloenzymes during the course of an enzymatic reaction (19). The binding of a substituted metal cofactor in the Mg^{2+}-binding site of an enzyme was demonstrated previously for the RNA helicase DbpA (20) and T7 DNA polymerase (21).

EXPERIMENTAL PROCEDURES

Materials

Oligonucleotides were obtained from Integrated DNA Technology. All chemical reagents and PP_i analogues were of molecular biology grade (Sigma). Nucleotides were purchased from Roche Applied Science. Radioactive materials were purchased from PerkinElmer Life Sciences. Acrylamide/bisacrylamide, 19:1 (40%), was purchased from Bio-Rad. The expression vectors used are pGP53 for wild type and the genetically modified T7 DNA polymerase deficient in 3′–5′-exonuclease activity. pGP53-D5D65 was a gift from Samir Hamdan (Harvard Medical School). pGP53-Δ28 was a gift from Stanley Tabor (Harvard Medical School). Wild-type and exonuclease-deficient T7 DNA polymerase were overproduced and purified using metal-free buffers as described previously (22).

Methods

Pyrophosphorolysis Assay—Degradation of a primer annealed to a DNA template by T7 DNA polymerase was measured in reactions containing various concentrations of PP_i (0, 0.4, 1.25, and 5 mM), 5 nM DNA primer-template (21-mer primer, 5′-CGAAACGACGGCCAGTGCCA-3′, and 26-mer template, 5′-CCCCTTGGCACTGGCCGTCGTTTTCG-3′), and 100 nM of T7 DNA polymerase in complex with thioredoxin (gp5-D5D5·trx and gp5Δ28·trx) in a buffer containing 40 mM Tris-HCl (pH 7.5), 10 mM $MgCl_2$, 10 mM DTT, and 50 mM potassium glutamate. For experiments using long primer-templates, we used the following DNA primer-template: 45-mer template, 5′-GGGAAAGTTGACGGGAGGGTATTGGAG-GTTAGTGGAGGTGAGTGG-3′; 45-mer primer for blunt duplex, 5′-…GTCAACTTTCCC-3′; 39-mer primer for recessed duplex, 5′-…GTCAAC-3′; 39-mer primer for bubble duplex, 5′-…CCTCGGCTCAAC-3′; 42-mer primer with three bases mismatch at the 3′ terminus (mismatch-3), 5′-…GTCAACAAA-3′; and 45-mer with six-base mismatch at the 3′ terminus (mismatch-6), 5′-…GTCAACAAAGGG-3′. After incubation at 37 °C for 20 min, the reaction was termi-

Downloaded from www.jbc.org at HARVARD UNIVERSITY, on August 13, 2011

nated by adding an equal volume of sample loading buffer containing 98% formamide, 0.1% bromphenol blue, and 20 mM EDTA. Unlabeled DNA primer (100 nM) was added, and the sample was heated prior to loading onto the gel. The samples were loaded onto 25% polyacrylamide gel for short DNA constructs (21-/26-mer duplex) and an 18% polyacrylamide gel for longer DNA oligonucleotides (39-/45-mer duplex) containing 3 and 7 M urea, respectively, and visualized using autoradiography after electrophoresis.

Analysis of the DNA product of pyrophosphorolysis requires radioactively labeled DNA primer. The DNA primer was labeled at its 5′-end using polynucleotide kinase and [γ-^{32}P]ATP at 37 °C for 20 min and was purified using BioSpin-6 columns (Bio-Rad). [^{32}P]PP_i was used in reactions for the identification of the dNTP products of the reaction in conjunction with unlabeled primer. Inorganic pyrophosphatase was added to the reaction to convert the PP_i to P_i, which is easier to distinguish from dNTP on the TLC plates. After incubation for 10 min at 37 °C, 0.4 μl from the reaction mixture was spotted onto a polyethyleneimine cellulose TLC plate (EMD) and developed using 0.5 M LiCl, 2 N acetic acid. At the end of the run, the plate was dried, and the radioactive products were visualized using autoradiography.

Determination of the Products of Pyrophosphorolysis and Pyrovanadolysis—Analysis of products of pyrophosphorylation and pyrovanadolysis required radioactive labeling of DNA substrate. DNA was labeled as follows: 10 μg of activated calf thymus DNA (Sigma) was incubated at 37 °C for 30 min in a 100-μl reaction containing 50 mM Tris-HCl (pH 7.2), 10 mM $MgSO_4$, 1 mM DTT, 0.5 mg/ml BSA, 32.5 μM of dNTPs, 50 μCi of [α-^{32}P]dGTP, and 20 units of DNA polymerase I. The labeled DNA was purified using BioSpin-6 columns (Bio-Rad). Pyrophosphorolysis or pyrovanadolysis was performed in an assay mixture containing 50 mM Tris-HCl (pH 7.5), 0.1 mM DTT, 50 mM NaCl, and 10 mM $MgCl_2$ or 1 mM $MnCl_2$, respectively. 0.2 μg of the labeled DNA was incubated at 37 °C for 20 min in a 10-μl reaction with T7 DNA polymerase (D5D65/trx), 3 mM dNTPs, 1 mM PP_i or VV, respectively. As a control, the labeled DNA was subjected to 3′–5′-exonuclease activity of wild-type T7 DNA polymerase. The pyrophosphorolysis or pyrovanadolysis reaction was stopped by the addition of 100 μl of a solution consisting of 0.6 ml of 1 M HCl, 0.1 M $Na_4P_2O_7$, 0.02 M KH_2PO_4, 0.2 ml of a Norit suspension (20% packed volume), and 0.1 ml of bovine serum albumin (5 mg/ml). The solutions were mixed and allowed to sit for 5 min at 0 °C. The mixture was applied to fiberglass filters, and the filters were washed with 1 M HCl, 0.1 M $NaPP_i$, and the retained radioactivity was determined. To probe whether phosphate is attached to the 5′-deoxynucleoside, the product was treated with 0.1 unit of 5′-nucleotidase from *Crotalus atrox* venom (Sigma) for 10 min at 37 °C.

Single Molecule Analysis of Strand Displacement Synthesis—Phage λ DNA (48.5 kb) molecules containing a replication fork were attached with the 5′-end of one strand to the glass surface of a flow cell via biotin-streptavidin link. The 3′-end of the strand is attached to a 2.8-μm paramagnetic bead (Dynal) via digoxigenin-anti-digoxigenin as described previously. To prevent nonspecific interactions between the beads and the surface, a 3-piconewton magnetic force was applied upward by positioning a permanent magnet above the flow cell. Beads were imaged with a CCD camera with a time resolution of 500 ms, and the centers of their positions for every acquisition time point were determined by particle-tracking software. Bead-bound and surface-tethered DNA were preincubated with 50 nM gp4 (hexameric concentration), 100 nM T7 DNA polymerase in buffer (40 mM Tris (pH 7.5), 50 mM potassium glutamate, 2 mM EDTA, 0.1 mg/ml BSA, and 1 mM pyrophosphate if indicated) consisting of 600 μM each of dATP, dTTP, dCTP, and dGTP, 10 mM DTT, 10 mM $MgCl_2$. Next, the flow cell was washed with replication buffer with dNTPs and DTT. Finally, DNA synthesis was initiated by introducing replication buffer with dNTPs, DTT, and 10 mM $MgCl_2$. For data analysis, after particle tracking, the traces were corrected for residual instabilities in the flow by subtracting traces corresponding to tethers that were not enzymatically altered. Bead displacements were converted into numbers of nucleotides synthesized using the known length difference between ssDNA and dsDNA at our experimental conditions.

X-ray Absorption Spectroscopy (XAFS) Assay

Sample Preparation for XAFS—The proteins were concentrated by centrifugation using Millipore Centricon (Bedford, MA) to yield a final concentration in the submillimolar range. The sample mixture contained gp5/trx (450 μM), primer-template (21-/26-mer duplex) DNA (sequence described above), and 300 μM Mn-PP_i or Mn-VV, respectively, in a buffer of 40 mM Hepes (pH 7.5), 50 mM potassium glutamate, 1 mM DTT, and 30% glycerol. The components were mixed at 0 °C and immediately frozen in copper sample holders (10 × 5 × 0.5 mm) covered with Mylar using liquid nitrogen. The sample cells were mounted in a Displex closed-cycle cryostat. To minimize thermal disorder and enhance signal-to-noise the temperature was kept at 20 K.

XAFS Data Collection—XAFS data collection was performed at the National Synchrotron Light Source at Brookhaven National Laboratory, beam line X3B. The spectra were recorded as described previously (23). The manganese K-edge was measured in a fluorescence mode at cryogenic temperature (20 K). The beam energy was selected using a flat Si(III) crystal monochromator with an energy resolution (dE/E): $\sim 2 \cdot 10^{-4}$. The incident beam intensity was recorded using a transmission ion chamber, and the fluorescence signal from the sample was measured using a 13-element germanium detector. For the calibration of the x-ray energy, the transmission signal of a MnO_2 foil reference was measured simultaneously with the sample fluorescence. For each sample, several scans were collected to obtain a total of 1×10^6 counts. The beam position was varied for each scan to minimize radiation damage, and samples were checked for visual signs of photoreduction (burn marks) after each scan (30 min). A further protection of the sample from radiation damage was obtained by using buffer containing 1 mM DTT to serve as a free radical scavenger. In addition, the protein sample was exposed to x-ray under cryogenic temperature. Examination of the samples on SDS-PAGE after the exposure to the x-ray beam revealed no evidence of protein degradation caused by radiation damage (data not shown).

Downloaded from www.jbc.org at HARVARD UNIVERSITY, on August 13, 2011

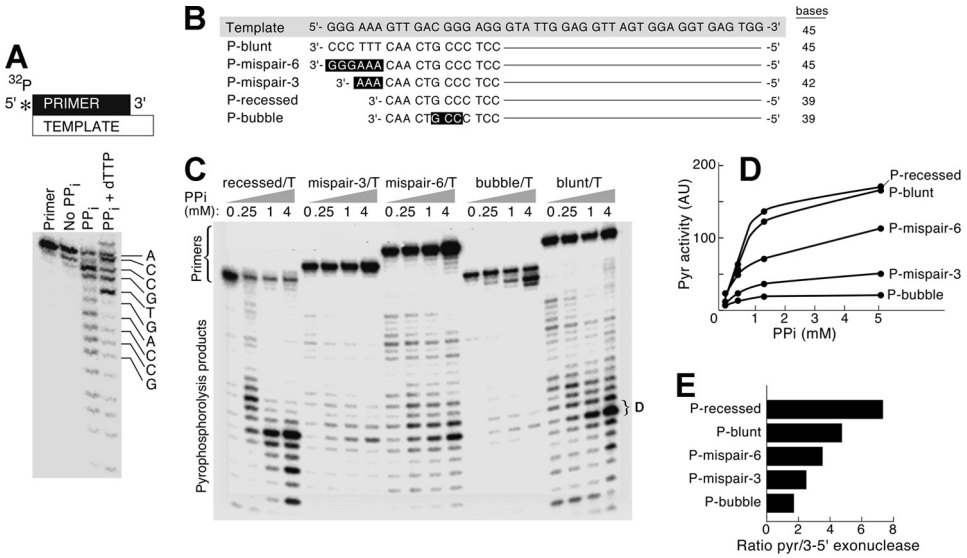

FIGURE 2. **Pyrophosphorolysis and pyrophosphate exchange.** *A,* gel analysis of pyrophosphorolysis catalyzed by T7 DNA polymerase. The reaction contained 100 nM T7 DNA polymerase deficient in the 3′–5′-exonuclease activity, 5 nM [5′-^{32}P]DNA primer (21-mer) annealed to template (26-mer), 40 mM Tris-HCl (pH 7.5), 10 mM $MgCl_2$, 10 mM DTT, 50 mM potassium glutamate, 250 μM PP_i, and 250 μM dTTP where indicated. After incubation at 37 °C for 20 min, the radioactive products were analyzed by electrophoresis through a 25% polyacrylamide gel containing 3 M urea and visualized using autoradiography. *1st lane,* 5′-^{32}P-labeled primer alone (no template); *2nd lane,* primer-template and no PP_i; *3rd lane,* primer-template and PP_i; *4th lane,* primer-template, PP_i, and dTTP. *B,* nucleotide sequences of the various DNA primers annealed to the same template. The primers are designated as follows: recessed, mispair-3, mispair-6, bubble (three mismatched bases), and blunt as indicated. *C,* effect of primer-template configuration on pyrophosphorolysis. The five primers described in *B* were incubated with T7 DNA polymerase and increasing amounts of PP_i as presented above. The products of the reaction were analyzed by electrophoresis through a 18% polyacrylamide gel containing 7 M urea and visualized using autoradiography. *D,* quantification of pyrophosphorolysis. The bands in the gels presented in *C* were analyzed using autoradiography. *E,* ratio of pyrophosphorolysis to exonuclease activity. The total intensities of the products in *lane 1* (no PP_i) and *lane 4* were quantified by integration of gel tracks the same as in *D*. The ratios between these lanes were calculated and represent the ratio of pyrophosphorolysis to exonuclease activity for each primer-template configuration.

XAFS Data Processing and Analysis—The average manganese K-edge absorption coefficient $\mu(E)$ was obtained after 4–5 independent XAFS measurements for each sample. To calibrate the x-ray energy, all spectra for each sample were aligned using the first inflection point of a reference MnO_2 foil x-ray absorption spectrum (6539 eV). The measured intensities were converted to $\mu(E)$, and the smooth pre-edge function was subtracted from the spectra to get rid of any instrumental background and absorption from other atomic edges. The data ($\mu(E)$) were normalized, and a smooth post-edge background function was removed to approximate $\mu(E)$ to isolate the EXAFS signal. The threshold E_0 was identified and was converted from energy to wave number space. The EXAFS signal was weighted and Fourier transformed to real space.

The XAFS data processing and the fitting to the EXAFS equation were performed using the iFEFFIT package (24, 25) as shown in Equation 1,

$$\chi(k) = \sum_j \frac{N_j f_j(k) e^{2k^2\sigma_j^2}}{kRj^2} \sin(2kR_j + \delta_j(k)) \qquad \text{(Eq. 1)}$$

where $f_j(k)$ and $\delta_j(k)$ are the scattering amplitude and the phase shift of the neighboring atom, respectively. Knowing these values, the distance to neighboring atom (R), the coordination numbers of neighboring atom (N), and the mean square disorder of neighbor distance (σ) were determined. Furthermore, based on scattering properties of the neighboring atoms, their atomic number (Z) value was also determined. This data analysis strategy, although employing chemical and physically reasonable constraints between the fitting parameters, provides general trends in the dynamic changes in coordination number and metal-ligand bond distances.

The same theoretical photoelectron path corresponding to the first shell Mn-O and second shell Mn-P/V distances were used to fit the datasets to examine different combinations of various Mn-O or Mn-P/V bond lengths for the first and second shell model. The input model was based on the crystallographic coordinates of T7 DNAP (PDB entry 1T8E). EXFAS analysis depends on the data points (K range and R range) to allow the determination of a limited number of parameters. The number of the variables to be determined in the process of EXAFS fitting must be smaller than the relevant independent points that are presented in the EXAFS spectrum (26). Therefore, to reduce the degrees of freedom of the fit, the following parameters were fixed for all data sets: the number of first shell ligands ($n = 6$) and the data range for fitting (Δr and Δk). The following parameters were varied: the correction to the photoelectron energy origin (ΔE_0), the relative movement of the O/P/V atom relatively to manganese (dr), and the mean square disorder of the corrections ΔR the Mn-O/Mn-P/V (σ^2). Therefore, the total number of variables was smaller than the number of independent data points in the experimental XAFS spectra. The best fit for each value of the starting phase fraction was found by locating the minimum of the statistical $\langle\chi\rangle^2$ values obtained in each fit.

RESULTS

Effect of Configuration of the Primer-Template on Pyrophosphorolysis—To establish optimal conditions for pyrophosphorolysis, we used a primer (21-mer) labeled with ^{32}P at its 5′ terminus annealed to a template (26-mer) (Fig. 2*A*). In these

Downloaded from www.jbc.org at HARVARD UNIVERSITY, on August 13, 2011

studies, we used a genetically modified T7 DNA polymerase *deficient* in its 3′–5′-exonuclease activity in complex with *E. coli* trx. Trx binds tightly to the polymerase to increase the processivity of polymerization of nucleotides (2). In this study, T7 DNA polymerase refers to the polymerase in complex with trx. The genetically modified T7 DNA polymerase (D5D65) has reduced levels of the 3′–5′-exonuclease activity that would normally hydrolyze the primers and complicate an analysis of the products of pyrophosphorolysis. Although the genetically altered polymerase has greatly reduced exonuclease activity (>1%), residual activity does remain. T7 DNA polymerase with a 28-residue deletion within the exonuclease domain (T7 gp5Δ28) has less than 0.1% the activity of wild-type polymerase, but this large deletion affects the polymerase activity (22). We have confirmed our pyrophosphorolysis and pyrovanadolysis results presented below using gp5Δ28 (data not presented). T7 DNA polymerase D5D65 and gp5Δ28 exhibit essentially the same pyrophosphorolytic and pyrovanadolytic activities. In this assay, pyrophosphorolysis results in the sequential degradation of the radioactively labeled primer with the release of dNTPs. The reaction can be monitored by gel analysis of the radioactively labeled primers. There is essentially no change in the length of the primer in the absence of PP_i, reflecting not only the absence of pyrophosphorolysis but also the relatively low exonuclease activity of the genetically modified T7 DNA polymerase (Fig. 2*A*, *2nd lane*). The addition of PP_i results in the appearance of a ladder of primers from 8 to 21 nucleotides in length (Fig. 2*A*, *3rd lane*). Addition of the next incoming nucleotide (dTTP) to the reaction mixture containing PP_i arrests T7 DNA polymerase at the only position on the DNA template suitable for dTMP incorporation (fifth nucleotide from the 3′-end of the primer, Fig. 2*A*, *4th lane*).

Different [5′-^{32}P]DNA primers (39–45-mer) annealed to the same DNA template (45-mer) were examined for their ability to support pyrophosphorolysis (Fig. 2*B*). These primers, after annealing to the template, resulted in primer-templates where the 3′-hydroxyl end of the primer is either recessed, blunt, unannealed, or located just distal to a bubble of three mismatched bases. The most efficient pyrophosphorolysis is obtained with either the recessed or the blunt configuration of the primer-template (Fig. 2, *C* and *D*). Those configurations with an imperfect match of the primer to the template were defective in supporting pyrophosphorolysis. Such a requirement for a properly annealed primer-template has been previously shown for *E. coli* DNA polymerase I (5) and for the *Sulfolobus solfataricus* DNA polymerase Dpo4 (7). Furthermore, a mismatch at the 3′ terminus of the primer renders its susceptible to the 3′–5′-exonuclease activity remaining in the genetically modified T7 DNA polymerase. Each lane on the gel contains a different number and intensity of degraded DNA bands (Fig. 2*C*). The first lane for each primer group represents the amount of nucleolytic cleavage by T7 DNA polymerase (no PP_i in the reaction mixture), and the other lanes represent the pyrophosphorolytic cleavage with increasing amounts of PP_i. The ratio of total intensities of the first to the fourth gel tracks indicates the relation between pyrophosphorolysis and exonuclease activity for each primer-template configuration (Fig. 2*E*). A perfectly matched primer-template assembly catalyzes pyrophosphorolysis more effectively than do the other primer-template configurations. The blunt end primer-template and the primer with six mismatched bases with the same DNA template (mispair-6) are subjected to nucleolytic degradation of the DNA in the absence of PP_i. The prominent nucleolytic degradation is due to the preference of the exonuclease activity for double-stranded DNA as shown previously (27). Interestingly, mispair-6 primer undergoes both enhanced nucleolytic degradation and enhanced pyrophosphorolytic activity relative to the primer with three mismatched bases and the primer with the bubble. The enhancement of both activities against the mispair-6 primer suggests that the mismatched primer must be sufficiently long to form a stable complex with sequences on the template strand.

PP_i Exchange—E. coli DNA polymerase I catalyzes an exchange reaction where pyrophosphate can exchange with the pyrophosphate present in a dNTP (5). PP_i exchange is thought to reflect pyrophosphorolysis in that the same structural requirements must be present in the primer-template (28). PP_i exchange activity occurs in the presence of the next incoming nucleotide, and the exchange of [^{32}P]PP_i with a dNTP is usually monitored. Each reaction mixture used to measure pyrophosphorolysis contains a primer (39-mer) annealed to a DNA template (45-mer), T7 DNA polymerase, $MgCl_2$, the same amount of [^{32}P]PP_i, and varying concentrations of PP_i. To better separate the [^{32}P]dNTP product from the [^{32}P]PP_i on thin layer chromatography plates, we coupled the reaction to pyrophosphatase. Pyrophosphatase hydrolyzes the excess [^{32}P]PP_i in the reaction to [^{32}P]P_i, which is readily distinguishable from [β,γ-^{32}P]dNTP (*see* "Experimental Procedures" and supplemental Fig. S1). An arrest of pyrophosphorolysis is observed upon addition of the next incoming dNTP (Fig. 2*A*, *4th lane*). In a reaction mixture containing PP_i and the next incoming nucleotide, there is an exchange of PP_i with the P_β–P_γ of the incoming nucleotide. The generation of product (dNTP) reveals that PP_i exchange by T7 DNA polymerase is slightly more rapid than is pyrophosphorolysis in the presence of Mg^{2+} (Fig. 3, *A* and *B*). When Mg^{2+} is substituted for Mn^{2+}, an increase of pyrophosphorolysis and PP_i exchange is observed (supplemental Fig. S1, *A* and *B*). The rate of PP_i exchange catalyzed by *E. coli* DNA polymerase I is higher than that of pyrophosphorolysis (29).

Effect of PP_i on Leading Strand Synthesis Observed at the Single Molecule Level—The observation of interactions of a single protein with a DNA molecule in real time provides information difficult to obtain with ensemble assays. T7 DNA polymerase and gene 4 helicase together mediate strand displacement synthesis with a processivity greater than 17,000 nucleotides per binding event (30).

We employed a single molecule DNA stretching assay to measure the effect of PP_i on the rate and processivity of the leading strand DNA synthesis (Fig. 3, *C* and *D*). In the absence of PP_i, T7 DNA polymerase and gp4 mediate strand displacement synthesis with the processivity of 15 ± 3 kb and the rate of 113 ± 1 bp/s. These values are in good agreement with the data that were previously reported (31). Addition of 1 mM PP_i to the reaction mixture results in a 40% decrease in the rate of leading strand synthesis (68 ± 1 bp/s). In our single molecule assay, we were able to observe the real time extension of the primer,

Downloaded from www.jbc.org at HARVARD UNIVERSITY, on August 13, 2011

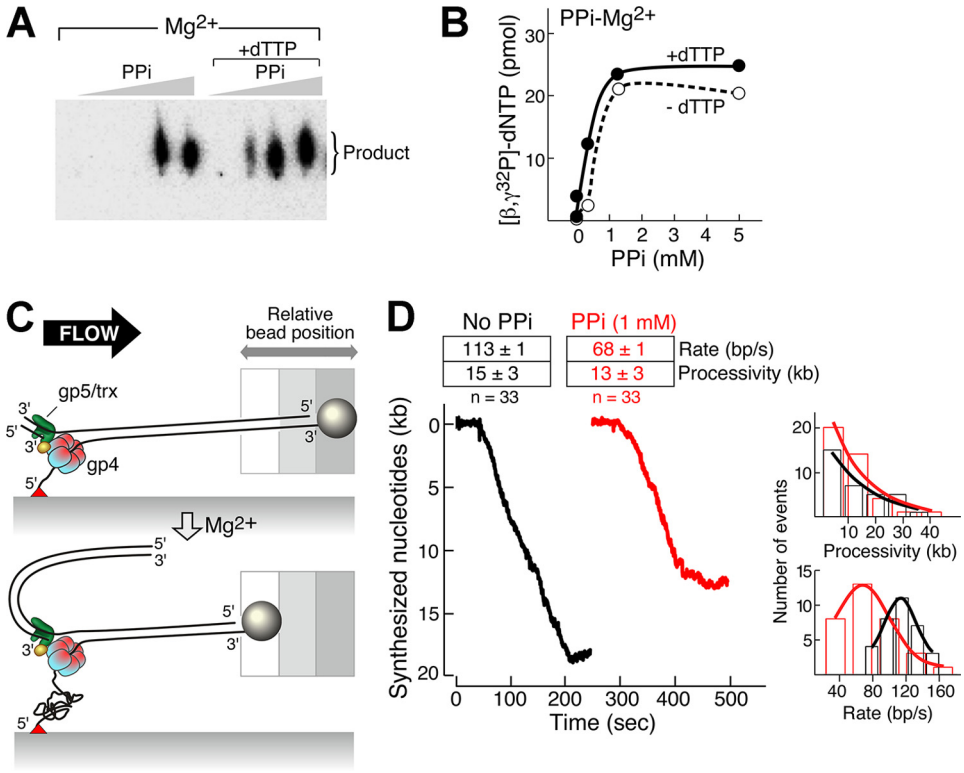

FIGURE 3. **Pyrophosphorolysis and PP_i exchange catalyzed by T7 DNA polymerase in bulk and at the single molecule level.** *A,* each pyrophosphorolysis reaction was performed as in Fig. 2*B* using the recessed primer annealed to the DNA template with the following modifications: same amount of [^{32}P]PP_i and varying amounts (0, 0.25, 1, and 4 mM) of PP_i in the absence or presence of 5 mM dTTP to induce pyrophosphorolysis or PP_i exchange. After incubation for 10 min at 37 °C 0.4 μl of the reaction mixture was spotted onto polyethyleneimine cellulose TLC plate and developed using 0.5 M LiCl, 0.5 M sodium formate. To better separate the [^{32}P]PP_i used in the reaction from the accumulated product ([^{32}P]dNTP), we coupled the reaction to pyrophosphatase (0.1 units). The radioactive products (dTTP) were visualized using autoradiography. *B, graphs* represent quantification of dNPPP formation from the pyrophosphorolysis reaction when increasing amounts of unlabeled PP_i are present. A full view on TLC is available in supplemental Fig. 3*A, top panel*. *C,* experimental design for the single molecule analysis of leading strand synthesis mediated by T7 DNA polymerase and gp4 helicase in the presence or absence of pyrophosphate. Duplex λ DNA (48.5 kb) is attached to the surface of the flow cell via the 5′-end of the fork using biotin-streptavidin interaction, and the 3′-end is attached to a paramagnetic bead using digoxigenin-anti-digoxigenin interaction. The replication reaction in the flow cell contains 50 nM gp4 (hexameric concentration), 100 nM T7 DNA polymerase in buffer consisting of 600 μM each of dATP, dTTP, dCTP, and dGTP, 10 mM DTT, 10 mM $MgCl_2$, and 1 mM pyrophosphate if indicated. DNA synthesis by proteins leads to conversion of the dsDNA to ssDNA, resulting in shortening of the DNA ligand that was accompanied by the movement of the bead against the direction of the flow. *D,* rate and processivity of leading strand synthesis by T7 DNA polymerase and gp4 helicase in the presence or absence of pyrophosphate. Examples of single molecule trajectories for leading strand synthesis are shown. Rate and processivity were calculated by fitting the distributions of individual single molecule trajectories using Gaussian and exponential decay distributions, respectively. Rate and processivity were calculated by fitting the distributions of individual single molecule trajectories using Gaussian and exponential decay distributions, respectively (fitted histograms shown are for gp5/trx and gp4 in the presence and the absence of 1 mM PP_i). Thirty three single events were used to calculate rate and processivity of the leading strand synthesis in the presence and the absence of pyrophosphate. Standard errors represent the accuracy in fitting of these distributions.

which in the presence of PP_i reflects the equilibrium between both pyrophosphorolysis and polymerization reactions. The measured rate of replication is likely the net value of two contributing rates that characterize pyrophosphorolysis and polymerization. It is important to emphasize that the addition of PP_i does not disturb the interactions between T7 DNA polymerase and gp4 helicase. Both proteins remain bound in a specific and stable complex as is reflected by the processivity of DNA synthesis. The processivity of leading strand synthesis measured in the presence of PP_i is equal to 13 ± 3 kb, which correlates well with the processivity of 15 ± 3 kb measured in the absence of PP_i.

Compounds That Mimic PP_i—As shown above, T7 DNA polymerase catalyzes pyrophosphorolysis on a recessed primer-template DNA in the presence of PP_i. We have examined compounds resembling pyrophosphate for their ability to support a pyrophosphorolysis-like reaction (Fig. 4). The compounds were selected on the basis of their charge and size and of the geometry of the oxygen that connects the two acyl groups in each molecule. The compounds examined are triphosphate, VV, phosphonoformate, and phosphonoacetate (Fig. 4*A*). Triphosphate has a different charge and size compared with PP_i. VV has a similar geometry and molecular structure as PP_i but very different chemical properties. Both phosphonoformate and phosphonoacetate have the potential to chelate divalent metal ions, such as Ca^{2+} and Mg^{2+}, to form stable coordinating compounds (9). These last two organophosphorous compounds inhibit the polymerase activity of several DNA polymerases, especially those encoded by viruses, and are used as antiviral agents (9). Both phosphonoformate and phosphonoacetate show high similarity to PP_i using the Superligand Database search.

In comparison with PP_i, none of these four compounds mediate an efficient pyrophosphorolysis-like reaction using the recessed primer annealed to a template in the presence of $MgCl_2$ (Fig. 4 and supplemental Fig. S2). However, when using 1 mM $MnCl_2$ instead of 10 mM $MgCl_2$, a sequential degradation of the primer is observed with VV but not with PP_i (Fig. 4*B*).

Downloaded from www.jbc.org at HARVARD UNIVERSITY, on August 13, 2011

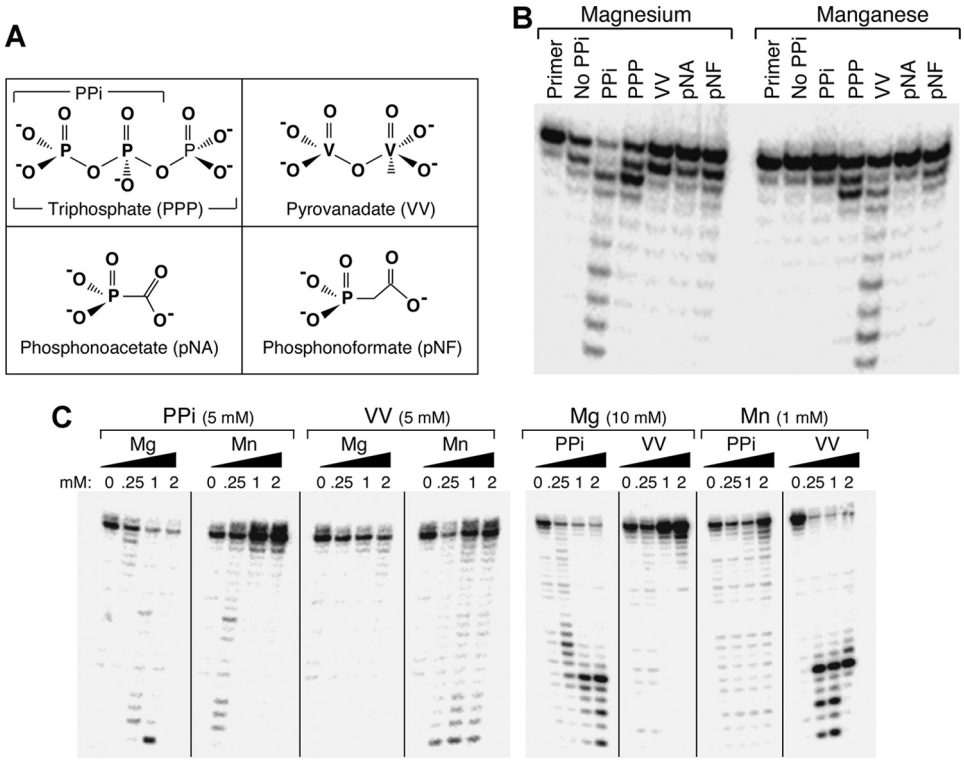

FIGURE 4. **Compounds that mimic PP_i.** *A,* compounds (triphosphate, VV, phosphonoformate, and phosphonoacetate) were selected on the basis of their charge, size, and geometry of the oxygen that connects the two acyl groups of PP_i. *B,* each of the compounds (250 μM) depicted in *A* were examined for their ability to mediate a pyrophosphorolysis-like reaction in the presence of 10 mM $MgCl_2$ or 1 mM $MnCl_2$, using the same primer-template DNA and reaction conditions as in Fig. 2*A*. *C,* effect of PP_i or VV on pyrophosphorolysis or pyrovanadolysis upon substitution of Mn^{2+} for Mg^{2+}. The reaction contained 5 mM PP_i or VV and increasing amounts of $MgCl_2$ or $MnCl_2$ (0, 0.25, 1, and 2 mM) (*left panel*) or 10 mM $MgCl_2$, 1 mM $MnCl_2$ and increasing amounts of PP_i or VV (0, 0.25, 1, and 2 mM) (*right panel*). The primer-template used consisted of the radiolabeled recessed primer as described in Fig. 2*B*. The reaction conditions and gel analysis of the products in *B* and *C* were otherwise as described in Fig. 2.

The optimal concentration of $MnCl_2$ for polymerization of nucleotides by T7 DNA polymerase is 1 mM (32). The same concentration of $MnCl_2$ is optimal for the pyrophosphorolysis-like activity observed with VV (Fig. 4*C* and supplemental Fig. S3). We designate this pyrophospholysis-like activity with VV pyrovanadolysis. The effect of PP_i and VV concentrations on pyrophosphorolysis and pyrovanadolysis in the presence of $MgCl_2$ (10 mM) and $MnCl_2$ (1 mM) is shown in Fig. 4*C* (*four left panels*). The effect of Mg^{2+} and Mn^{2+} concentration on pyrophosphorolysis and pyrovanadolysis is presented in Fig. 4*C* (*four right panels*). Pyrophosphorolysis requires a higher concentration of Mg^{2+} in comparison to Mn^{2+}, whereas pyrovanadolysis relies exclusively on the presence of Mn^{2+} (supplemental Fig. S3).

Comparison of Pyrophosphorolysis and Pyrovanadolysis—After we observed the degradation of DNA primer by VV in a pyrophosphorolysis-like manner, we probed the nature of the product of pyrovanadolysis using radioactively labeled DNA (see under "Experimental Procedures") (Fig. 5*A*). Upon incubation with PP_i and Mg^{2+}, a radioactive product is formed (Fig. 5*B*, *lane 4*) with a mobility on TLC plates similar to dGTP; the primer strand was radioactively labeled with [^{32}P]dGMP (Fig. 5*B*, *lane 1*). In the presence of VV and Mn^{2+}, this product is not observed, and a distinct and more rapidly migrating product is observed (Fig. 5*B*, *lane 5*). The product of pyrovanadolysis has the same mobility on TLC plates as dGMP (Fig. 5*B*, *lane 3*). The radioactive product of pyrovanadolysis is adsorbed by activated charcoal as expected for a nucleotide (data not shown). VV was identified at the bottom of the TLC plate by the appearance of a green spot under reducing conditions and low pH, conditions under which vanadium turns this distinct color (Fig. 5*B*, *right panel* representing the visible *green spot* in natural light at the *bottom* of *lane 5*).

To ensure that phosphate is attached to the 5′-deoxynucleoside formed in pyrovanadolysis, the product was treated with 5′-nucleotidase from *C. atrox* venom (Sigma). 5′-Nucleotidase is specific for a nucleoside 5′-monophosphate. The product of pyrovanadolysis was incubated with 5′-nucleotidase, and as a result the radioactive product adsorbed by activated charcoal was decreased to 20% of the product absorbed in the absence of nucleotidase treatment. The decrease in adsorbed ^{32}P indicates that at least 80% of the product of pyrovanadolysis is dGMP. Using reaction conditions as in Fig. 3, *A* and *B,* we show that VV competes with PP_i for the binding to the active site through either Mg^{2+} or Mn^{2+} (supplemental Fig. S4, *A–C*), but it fails to inhibit completely pyrophosphorolysis, indicating that the binding affinity of Mn^{2+} to VV is lower than to PP_i.

The identification of dGMP, rather than dGPVV, as the product of pyrovanadolysis is not surprising in that the V–OR bond is more covalent than the P–OR bond. The increased stability results in a more labile anhydride group (ROV–O–P). Density functional theory calculations have shown that the formation of a vanadate ester adduct in the active site of DNA polymerase is not favorable (33).

Downloaded from www.jbc.org at HARVARD UNIVERSITY, on August 13, 2011

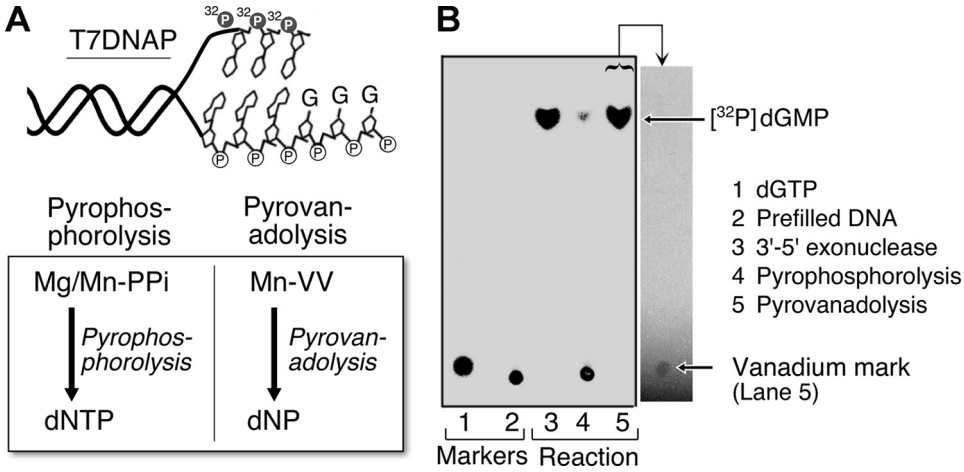

FIGURE 5. **Identification of products of pyrophosphorolysis and pyrovanadolysis.** *A,* schematic representation of the DNA substrate with the 3′-labeled primer strand. The substrate was prepared by using T7 DNA polymerase (*T7DNAP*) to add [^{32}P]dGMP to the 3′ terminus of the primer strand as described under "Experimental Procedures." *B,* pyrophosphorolysis and pyrovanadolysis were catalyzed by T7 DNA polymerase using 5 mM PP_i or VV, respectively, in a reaction containing the radioactively labeled DNA depicted in *A*. $MgCl_2$ (10 mM) was used in the reaction containing PP_i and $MnCl_2$ (1 mM) in the reaction containing VV. *Lane 1* contains only [α-^{32}P]dTTP as a marker. *Lane 2,* only DNA substrate. *Lane 3,* reaction mixture without PP_i or VV containing 10 mM $MgCl_2$ and T7 DNA polymerase (wild type). *Lane 4* contains reaction mixture with genetically modified T7 DNA polymerase (gp5-D5D65/trx), $MgCl_2$, and PP_i. *Lane 5* contains reaction mixture with genetically modified T7 DNA polymerase, $MnCl_2$, and VV. The products of exonuclease activity, pyrophosphorolysis, and pyrovanadolysis were visualized using TLC and developed in 0.5 M LiCl and 2 N acetic acid and analyzed using autoradiography.

Structural Analysis of the Active Site of T7 DNA Polymerase Using X-ray Absorption Spectroscopy—Nucleotide incorporation engages sequential steps involving interaction of the polymerase with both the incoming dNTP and the primer-template, events associated with conformational changes in the active site (34). We have used XAFS to examine the structural changes occurring at the active site upon binding of PP_i and VV. XAFS is a powerful technique used to probe the metal-binding site of metalloproteins (35). Analysis of the x-ray absorption spectra provides high resolution structural and electronic information of the metal site and can measure the transition core electronic states of the metal ion. The active site of DNA polymerase contains two Mg^{2+} ions and thus is well suited for XAFS analysis. To demonstrate that most of the Mn^{2+} is complexed with the enzyme and does not remain free in solution, we used a site-directed titration approach using XAFS (21). Binding of adenosine nucleotides to the active site of T7 DNA polymerase was achieved by titration of the polymerase above and below its binding constant to dNTP (K_d = 20 μM (36)). The protein/nucleotide ratios were calculated based on the desired complex concentration and the equilibrium dissociation constant for the protein-ligand binding equilibria (21).

To study the structural basis for pyrophosphorolysis and pyrovanadolysis in greater detail, we prepared identical samples of Mn^{2+}-substituted T7 DNA polymerase with either PP_i or with VV. We then analyzed the metal-binding site using XAFS. A more detailed XAFS analysis was aimed at probing the confined structural properties of the metal-PP_i /VV interactions with the enzyme. Standard curve fitting was performed using the iFeffit package (24) for the real and imaginary parts of the Fourier-transformed $\chi(k)$ (Fig. 6*A*). We compared the structure of the metal-binding site of T7 DNA polymerase when bound to Mn-PP_i or to Mn-VV (Fig. 6*A*). The available crystal structure of T7 DNA polymerase (PDB code 1T8E) was used as a model for the fitting analysis. The oscillations for the PP_i- and VV-bound states of DNA polymerase were fitted over the magnitude of the photoelectron wave number region of 2.5–10 ($Å^{-1}$). The EXAFS fitting results are summarized in Table 1. Analysis of the EXAFS data (Table 1) shows that the distances of the first shell atoms from Mn(O) remain similar (2.2–2.3 Å) whether PP_i or VV is bound to the active site. The phase differences of the metal-substituted EXAFS spectra (Fig. 6*A*, *inset*) can be attributed to a combination of the differences in the absorbers' phase shift with Z and the arbitrary assignment of the ionization threshold, E_0, which is the basis for calculating the wave vector magnitude from the energy.

The similarity in frequency of the spectra of the PP_i-bound state compared with the VV-bound state of T7 DNA polymerase (Fig. 6*A*, *insets*) attests to a corresponding relative similarity in absorber nearest-neighbor distance for the examined metal ion cofactor. The EXAFS differences between the PP_i- and the VV-bound states of manganese-substituted DNA polymerase are due to the high electron density of vanadium compared with that of phosphorus. The major peak observed in the Fourier transforms of the EXAFS for the DNA polymerase samples (Fig. 6*A*) is due to the backscattering amplitude of oxygen atoms. The second coordination shell peak of the VV-bound state (Fig. 6*A*, *bottom*) corresponds to the two vanadium atoms and is more pronounced than is the peak attributed to the two phosphorus atoms in the second coordination shell of the PP_i bound to polymerase (Fig. 6*A*, *top*). Structural changes in the active site of T7 DNA polymerase certainly play a critical role upon binding of PP_i or VV and the preference for metal cofactor in pyrophosphorolysis or pyrovanadolysis. The distance of the second shell phosphorus atoms from the absorber (manganese) is shorter upon PP_i binding than upon ddATP binding (Fig. 6*B*). However, upon binding of VV, the distance of Mn^{2+} from the second shell vanadium atoms is shorter compared with the distance of the phosphorus atoms in either PP_i or ddATP (Fig. 6*B*).

Downloaded from www.jbc.org at HARVARD UNIVERSITY, on August 13, 2011

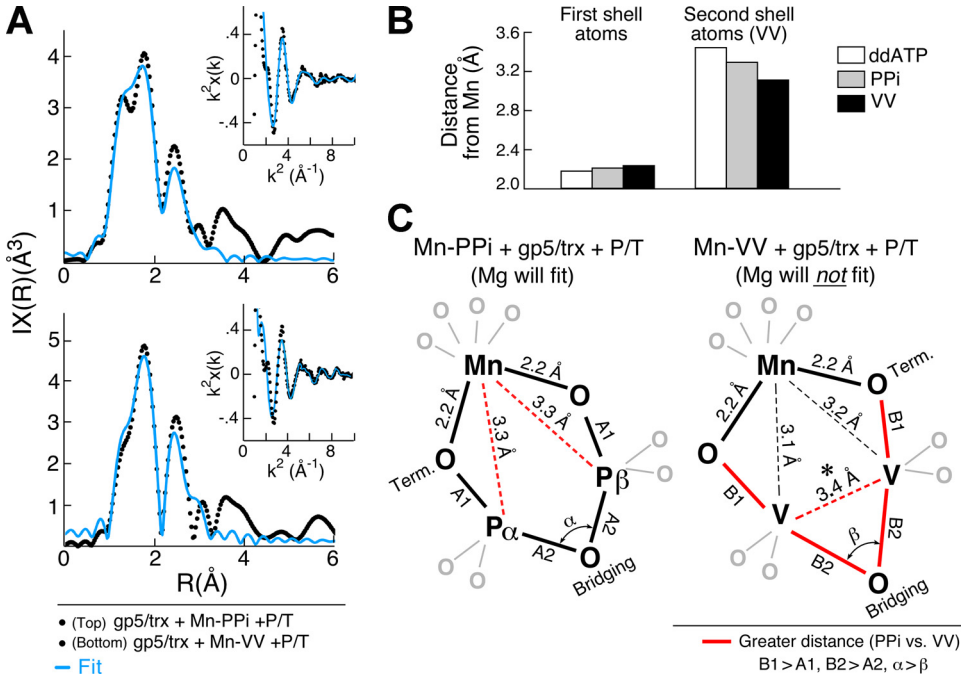

FIGURE 6. **Distance distribution of PP_i, VV, and protein ligands around the manganese in the active site of T7 DNA polymerase.** *A,* EXAFS fitting results of T7 DNA polymerase. Manganese K-edge EXAFS data (*inset*) and its Fourier transform in real space for PP_i (*top*) or VV (*bottom*) bound in the active site of T7 DNA polymerase. Best fits (*cyan*) to the experimental data (*black*) are indicated. EXAFS analysis was performed using the iFFEFIT analysis package. The theoretical EXAFS signal was constructed of the bacteriophage T7 DNA polymerase (PDB entry 1T8E) and calculated using FEFF embedded in the iFFEFIT package (24, 25). *B,* columns representing the Mn-O, Mn-P, and Mn-V coordination bond distances based on EXAFS fitting results. The fitting parameters are summarized in Table 1. *C,* schematic representation of T7 DNA polymerase active site configuration when bound to Mn- PP_i and Mn-VV, respectively. Bond distances were obtained from EXAFS results summarized in Table 1 (*black*). The distances of terminal and bridging oxygens in phosphorus or vanadium and the angle of bridging oxygen (POP and VOV) is based on available crystal structures of PP_i and VV free or bound to an enzyme active site (summarized in supplemental Table 1).

TABLE 1

Analysis of EXAFS data

EXAFS curve fitting results are shown for the Mn^{2+}-substituted T7 DNA polymerase bound to PP_i and VV. Sample preparation is described under "Experimental Procedures." Mn-O and Mn-P/V represent the different first and second shell bond distance in the model. The best fit for DNA polymerase was obtained using a two atoms model (oxygen and phosphorus or vanadium). The local structure around manganese was taken from the crystal structure of T7 DNA polymerase and used as the model for the curve fitting. Mg^{2+} was substituted with Mn^{2+}, and the theoretical scattering factors were calculated using FEFF module embedded in the iFEFFIT package (25). χ^2 stands for the goodness of fit; *R* indicates the distance of protein/compound ligands from manganese in angstroms; E_0 indicates the correction to the energy origin; and σ is the Debye-Waller factor. P/T indicates primer-template.

			Mn-O (X6)			Mn-P (X2)		
	χ^2	R factor	R (Å)	E_θ	σ^2	R (Å)	E_θ	σ^2
Mn-PPi + T7 DNA polymerase + P/T	7.14	0.006	2.22 ± 0.04	0.03	0.015	3.26 ± 0.06	0.03	0.004
						3.34 ± 0.06	0.03	0.004

			Mn-O (X6)			Mn-V (X2)		
	χ^2	R factor	R (Å)	E_θ	σ^2	R (Å)	E_θ	σ^2
Mn-VV + T7 DNA polymerase + P/T	5.74	0.008	2.24 ± 0.06	2.02	0.006	3.09 ± 0.12	2.02	$1.5X10^{-4}$
						3.17 ± 0.12	2.02	$1.5X10^{-4}$

DISCUSSION

In this study, we show that T7 DNA polymerase catalyzes pyrophosphorolysis and PP_i exchange in a manner similar to that found for *E. coli* DNA polymerase I (29). In pyrophosphorolysis, PP_i attacks the 3′-end of a primer properly annealed to a template to release dNTPs in a stepwise fashion (Fig. 7*A*) (5). If the next incoming dNTP is present, there is an exchange of PP_i with the β,γ-phosphates of the nucleotide. PP_i exchange reflects a transient step in pyrophosphorolysis and represents a dynamic transition between the hydrolysis of the β,γ-phosphate linkage and the condensation of PP_i with dNMP. PP_i exchange has no known biological significance and is possibly a side effect of pyrophosphorolysis according to the law of mass action. Pyrophosphorolysis under some circumstances, however, could serve a function similar to that of the 3′–5′-exonuclease activity associated with DNA polymerases (7). Indeed, the accumulation of PP_i during DNA sequencing reactions results in the selective removal of the chain terminating dideoxynucleotides from oligonucleotides (8). Pyrophosphorolysis catalyzed by HIV-1 reverse transcriptase can remove chain-terminating zidovudine from the 3′ terminus of a DNA primer (37). Using a single molecule approach, we show that PP_i reduces the rate of leading strand synthesis by T7 DNA polymerase and gp4 helicase but leaves the processivity unchanged. The decrease in the rate of leading strand synthesis in the presence of PP_i strengthens the conclusion that pyrophosphorolysis occurs at the active site.

The large fragment of the *E. coli* polymerase I (Klenow fragment) shares the high sequence homology with T7 DNA polymerase (29). Therefore, we expected that Mn^{2+} could replace Mg^{2+} for pyrophosphorolysis catalyzed by T7 DNA polymerase as was observed for the Klenow fragment. Mn^{2+} can also replace Mg^{2+} for pyrophosphate exchange by T7 DNA polymerase with the same requirements found for pyrophosphorolysis. As in the polymerization reaction, T7 DNA polymerase requires a significantly lower amount of

Downloaded from www.jbc.org at HARVARD UNIVERSITY, on August 13, 2011

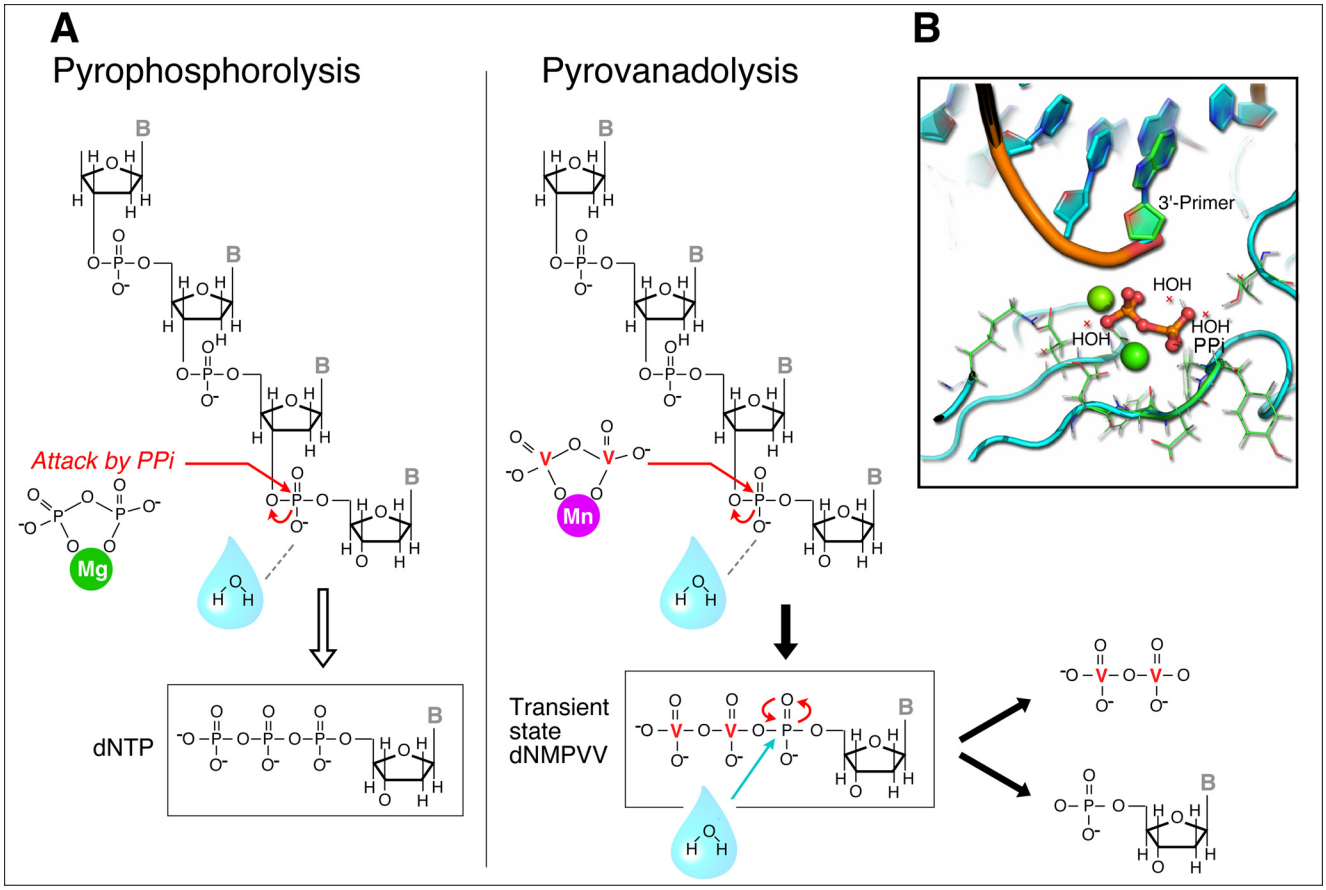

FIGURE 7. **Molecular model of pyrophosphorolysis and pyrovanadolysis.** *A,* proposed mechanism for pyrophosphorolysis (*left panel*) and pyrovanadolysis (*right panel*). In pyrophosphorolysis PP_i attacks the phosphate backbone of the 3′-end of the primer to yield dNTP. A water molecule may stabilize the 3′-end of the primer and make it a better leaving group. In pyrovanadolysis the formation of dNMPVV is transient and is followed by attack of water molecule that breaks the phosphovanadate bond to yield dNMP. *B,* in the active site of Dpo4 two water molecules are observed in close proximity to the primer.

Mn^{2+} in comparison with Mg^{2+} for both pyrophosphorolysis and PP_i exchange.

The similarity of vanadate and phosphate chemistry raised the question as to whether VV could mediate a pyrophosphorolysis-like reaction. Indeed, VV can replace PP_i when Mn^{2+} is substituted for Mg^{2+}. What is the mechanism of pyrovanadolysis and why is there a requirement for Mn^{2+} rather than for Mg^{2+}? The chemical similarity of vanadate to phosphate (13) enables it to compete with phosphate in reactions catalyzed by many enzymes associated with phosphate metabolism. The chemical reservoirs of biochemical energy are phosphates (38), and these compounds predominate in biochemical processes. Like phosphate, vanadate can serve as a bridge between two nucleotides and still remain charged. However, the low potential energy stored in a phosphovanadate bond (2–3 kcal/mol) compared with that of a phosphodiester bond (7 kcal/mol, as in dNTP) and the low abundance of vanadate in nature make it a poor candidate for providing energy for biological processes. We could not directly detect deoxyribonucleoside monophosphate divanadate (dNPVV) as a product but only deoxyribonucleoside monophosphate (dNMP). Most probably, dNPVV undergoes hydrolysis. The V-OR bond is more covalent than the P-OR bond rendering the anhydride group ROV–O–P more prone to hydrolysis than ROP–O–P (39). Vanadate forms mixed anhydride with phosphate and arsenate as analogues of pyrophosphate and triphosphate (16).

Our EXAFS data clearly show the similarity to pyrophosphate binding, making it most likely that the active species is indeed divanadate. Even so, the detection of the dNPVV remains elusive because of its lability, and we clearly show that pyrovanadolysis is a pyrophosphorolysis-like reaction, and the proposed mechanism is the most likely based on the current experimental data.

It was shown previously that RNA polymerase can catalyze a pyrophosphorolysis-like reaction when arsenate-containing compounds similar to PP_i were used as follows: methylene-bis-arsenate, arseno-methylphosphonate, and arsenoacetate (10). The product of such pyrophosphorolysis-like activity by RNA polymerase was ribonucleoside monophosphate but not any arseno-derivative of nucleoside triphosphate. The formation of dNMP in the pyrovanadolysis reaction by T7 DNA polymerase could arise by the attack of a water molecule on dNPVV to hydrolyze the phosphovanadate bond (Fig. 7*A*.). The structure of the active site of *S. solfataricus* P2 DNA polymerase (Dpo4) reveals the presence of two water molecules in close proximity to the primer (Fig. 7*B*).

In our attempt to chemically synthesize deoxythymidine monophosphate divanadate, we used variations of Eckstein's

Downloaded from www.jbc.org at HARVARD UNIVERSITY, on August 13, 2011

method and a modification of the $POCl_3$ method used to synthesize dNTP (40–42). Both methods involve using pyrovanadate to attack an activated phosphate ester on the 5′-position of thymidine. In these reactions, the initial steps are carried out under anhydrous conditions; however, the final step and purification are in the presence of water. We believe that it is at this point that water hydrolyzes the deoxythymidine monophosphate divanadate to yield dTMP, as we were only able to isolate dTMP after HPLC purification.

Vanadate undergoes nonenzymatic condensation with phosphate ligands (43) to yield a rapid and thermodynamically favorable formation of phosphovanadate anhydrides (16). The formation constant of phosphovanadate is 20 times higher than is the formation constant of pyrophosphate from two monophosphate molecules. Therefore, we anticipated that an enzyme that usually forms phosphodiester bonds would be able to catalyze the condensation reaction to yield dNPVV. Pyrovanadolysis does indeed occur but only with the substitution of Mn^{2+} for Mg^{2+}, a metal that does not support pyrophosphorolysis under the same reaction conditions. Mn^{2+} probably stabilizes the reactive state of VV and favors the attack of the primer. It is possible that Mn^{2+} functions as an electron sink that lowers the electrophilic ability of the VV, making it a better substrate.

The only enzyme known to be activated by VV is phosphoglycerate mutase (17). The two charged vanadate moieties occupy the binding loci for the carboxylate and phosphate of the monophosphoglycerate in the active site of the enzyme. The only crystal structure available for an enzyme bound to VV is of YopH, a tyrosine phosphatase produced by a pathogenic *Yersinia* species (18). In comparison with YopH, there are 119 crystal structures of proteins bound to PP_i available in the PDB. The structure of YopH demonstrates how a mutation in the hinge region impairs catalytic activity and reveals a unique transition state-like structure of VV (18).

Although the geometry and electronic structure of PP_i and VV are similar, their chemical properties are quite different. The differences in PP_i and VV free or bound to Dpo4 and YopH, respectively, are summarized in supplemental Table S1. The mean bond lengths between the oxygen atoms and the central atoms are 1.52 Å (terminal) and 1.59 Å (bridging anhydride) if phosphorus is the central atom (44), and 1.69 Å (terminal) and 1.8 Å (bridging) if vanadium is the central atom (45). The angle of OPO (144°), as determined from crystals of MgP_2O_7 (44) is larger than that of OVO (141°) in crystals of MgV_2O_7 (45). Furthermore, the chemical properties of vanadium differ from those of phosphorus. Vanadium is a transition metal ion and bears a different electronic arrangement than does phosphorus. 1) The atomic radius of vanadium is bigger than that of phosphorus. 2) Vanadium can be penta/hexa-coordinated, whereas the coordination state of phosphate is tetrahedral. 3) Oxidation potentials are different; oxidation states for vanadium compounds range from −1 to 5 (considered as amphoteric oxide), whereas the oxidation states for phosphorus compounds range from −3 to 5 (considered as mildly acidic oxide).

During pyrophosphorolysis and pyrovanadolysis, the metal ion coordinates through the nonbridging oxygens of PP_i and VV. Therefore, the relative size and shape of both VV and of the metal in the active site of DNA polymerase are important. We have examined the inter-atomic distances of the surrounding ligand atoms in the polymerase active site upon binding of PP_i or of VV. Combining the EXAFS fitting results with prior knowledge of the bridging vanadium/phosphorus-oxygen bond length and the terminal vanadium/phosphorus-oxygen bond length (supplemental Table S1) enabled us to build a structural model. The larger structure of VV explains the need for Mn^{2+} to fit into the active site of T7 DNA polymerase to catalyze pyrovanadolysis (Fig. 6*C*).

The prominent differences in the higher shell XAFS spectra of the Mn^{2+}-substituted polymerase indicate a different spatial arrangement of the active site upon binding of VV. The difference in spatial arrangement between VV and PP_i bound to the active site of T7 DNA polymerase is associated with the fine geometry of higher coordination shells, as indicated by the Fourier transform XAFS analysis. Based on the phosphorus or vanadium contribution to the spectrum by PP_i or VV, we attempted to fit the next nearest neighbor atomic shells at ~3–4 Å. The XAFS results shed light on the structural basis of the Mn^{2+}-mediated pyrophosphorolysis. It is clear that Mn^{2+}-mediated pyrovanadolysis by T7 DNA polymerase has a structural origin.

Pyrophosphorolysis is initiated by withdrawing an electron from the reaction center. The most important part in such electrophilic catalysis is the formation of a substrate-metal complex (46). The subsequent catalysis involves donation of a proton from the solvent via the metal to the phosphate backbone of the primer as well as an electron sink involving side chains of residues in the active site. The electronic structure, oxidation potential, and the size of the metal cofactor play an important role whereby the metal ion can catalyze the reaction as indicated by a preference of Mn^{2+} over Mg^{2+}. In the two-metal-ion mechanism for nucleotide condensation catalyzed by polymerases (4), the catalytic Mg^{2+} binds to the primer and prepares the 3′-hydroxyl for the nucleophilic attack by PP_i. The structural Mg^{2+} stabilizes and enhances the nucleophilicity of the hydroxyl group. Because pyrophosphorolysis is a reversal of the polymerization reaction, this mechanism and the two metal ions must also be invoked in pyrophosphorolysis.

T7 DNA polymerase, unlike most other members of the polymerase I family, does not discriminate against chain terminating ddNTPs (32, 47, 48). The lack of discrimination against ddNTPs arises from the presence of a tyrosine at position 526 in the nucleotide-binding pocket (48). Replacement of this tyrosine with phenylalanine, a residue found in the corresponding position in *E. coli* DNA polymerase I, leads to a several hundredfold discrimination against the incorporation of dideoxynucleotides (48). The substitution of Mn^{2+} for Mg^{2+} reduces discrimination against ddNTPs by T7 DNA polymerase and reduces discrimination about 4-fold in *E. coli* DNA polymerase I (32). To determine whether the Y526F mutation alters the preference for Mn^{2+} in pyrovanadolysis, we examined the ability of polymerase-Y526F to catalyze pyrovanadolysis. The Y526F modification has no significant effect on pyrophosphorolysis or PP_i exchange (supplemental Fig. S5*A*). Mn^{2+} does not alter the selectivity of PP_i using polymerase-Y526F suggesting that Tyr-526 is involved in the

Downloaded from www.jbc.org at HARVARD UNIVERSITY, on August 13, 2011

release of PP_i through binding to the Pβ (3) but is less important for the binding of PP_i (supplemental Fig. S5*B*). However, other residues in proximity to the terminal oxygen of PP_i may play a role in switching between the forward and reverse activities (supplemental Fig. S5*C*).

Acknowledgments—We thank Michael Sullivan, Jennifer Bohon, and Donald Abel (Beamline X-3B, National Synchrotron Light Source, Upton, NY) for technical support. We thank Ingrid Richardson and Dr. Meni Wanunu for critical reading of the manuscript and Prof. Dieter Rehder and Dr. Stanley Tabor for helpful discussions.

REFERENCES

1. Hamdan, S. M., and Richardson, C. C. (2009) *Annu. Rev. Biochem.* **78,** 205–243
2. Tabor, S., Huber, H. E., and Richardson, C. C. (1987) *J. Biol. Chem.* **262,** 16212–16223
3. Doublié, S., Tabor, S., Long, A. M., Richardson, C. C., and Ellenberger, T. (1998) *Nature* **391,** 251–258
4. Steitz, T. A. (1998) *Nature* **391,** 231–232
5. Deutscher, M. P., and Kornberg, A. (1969) *J. Biol. Chem.* **244,** 3019–3028
6. Heinonen, J. K. (2001) *Biological Role of Inorganic Pyrophosphate*, p. 10, Kluwer Academic Publishers, Boston
7. Vaisman, A., Ling, H., Woodgate, R., and Yang, W. (2005) *EMBO J.* **24,** 2957–2967
8. Tabor, S., and Richardson, C. C. (1990) *J. Biol. Chem.* **265,** 8322–8328
9. Griengl, H., Hayden, W., Penn, G., De Clercq, E., and Rosenwirth, B. (1988) *J. Med. Chem.* **31,** 1831–1839
10. Rozovskaya, T. A., Rechinsky, V. O., Bibilashvili, R. S., Karpeisky, MYa, Tarusova, N. B., Khomutov, R. M., and Dixon, H. B. (1984) *Biochem. J.* **224,** 645–650
11. Wolfe-Simon, F., Switzer Blum, J., Kulp, T. R., Gordon, G. W., Hoeft, S. E., Pett-Ridge, J., Stolz, J. F., Webb, S. M., Weber, P. K., Davies, P. C., Anbar, A. D., and Oremland, R. S. (2011) *Science* **332,** 1163–1166
12. Fekry, M. I., Tipton, P. A., and Gates, K. S. (2011) *ACS Chem. Biol.* **6,** 127–130
13. Crans, D. C., Smee, J. J., Gaidamauskas, E., and Yang, L. (2004) *Chem. Rev.* **104,** 849–902
14. Tracey, A. S., and Gresser, M. J. (1986) *Proc. Natl. Acad. Sci. U.S.A.* **83,** 609–613
15. Steens, N., Ramadan, A. M., and Parac-Vogt, T. N. (2009) *Chem. Commun.* **8,** 965–967
16. Gresser, M. J. (1986) *J. Am. Chem. Soc.* **108,** 6229–6234
17. Stankiewicz, P. J., Gresser, M. J., Tracey, A. S., and Hass, L. F. (1987) *Biochemistry* **26,** 1264–1269
18. Brandão, T. A., Robinson, H., Johnson, S. J., and Hengge, A. C. (2009) *J. Am. Chem. Soc.* **131,** 778–786
19. Solomon, A., Akabayov, B., Frenkel, A., Milla, M. E., and Sagi, I. (2007) *Proc. Natl. Acad. Sci. U.S.A.* **104,** 4931–4936
20. Akabayov, B., Doonan, C. J., Pickering, I. J., George, G. N., and Sagi, I. (2005) *J. Synchrotron Radiat.* **12,** 392–401
21. Akabayov, B., and Richardson, C. C. (2011) *Powder Diffraction* **26,** 159–163
22. Tabor, S., and Richardson, C. C. (1989) *J. Biol. Chem.* **264,** 6447–6458
23. Akabayov, B., Lee, S. J., Akabayov, S. R., Rekhi, S., Zhu, B., and Richardson, C. C. (2009) *Biochemistry* **48,** 1763–1773
24. Newville, M. (2001) *J. Synchrotron Radiat.* **8,** 322–324
25. Ravel, B., and Newville, M. (2005) *J. Synchrotron Radiat.* **12,** 537–541
26. Stern, E. A. (1993) *Phys. Rev. B Condens. Matter* **48,** 9825–9827
27. Andraos, N., Tabor, S., and Richardson, C. C. (2004) *J. Biol. Chem.* **279,** 50609–50618
28. Gabbara, S., and Peliska, J. A. (1996) *Methods Enzymol.* **275,** 276–310
29. Kornberg, A., and Baker, T. A. (1992) *DNA Replication*, p. 115, W. H. Freeman & Co., New York
30. Lee, J. B., Hite, R. K., Hamdan, S. M., Xie, X. S., Richardson, C. C., and van Oijen, A. M. (2006) *Nature* **439,** 621–624
31. Akabayov, B., Akabayov, S. R., Lee, S. J., Tabor, S., Kulczyk, A. W., and Richardson, C. C. (2010) *Proc. Natl. Acad. Sci. U.S.A.* **107,** 15033–15038
32. Tabor, S., and Richardson, C. C. (1989) *Proc. Natl. Acad. Sci. U.S.A.* **86,** 4076–4080
33. Borden, J., Crans, D. C., and Florián, J. (2006) *J. Phys. Chem. B* **110,** 14988–14999
34. Patel, P. H., and Loeb, L. A. (2001) *Nat. Struct. Biol.* **8,** 656–659
35. Scott, R. A., Schwartz, J. R., and Cramer, S. P. (1985) *J. Inorg. Biochem.* **23,** 199–205
36. Patel, S. S., Wong, I., and Johnson, K. A. (1991) *Biochemistry* **30,** 511–525
37. Arion, D., and Parniak, M. A. (1999) *Drug Resist. Updat.* **2,** 91–95
38. Westheimer, F. H. (1987) *Science* **235,** 1173–1178
39. Krauss, M., and Basch, H. (1992) *J. Am. Chem. Soc.* **114,** 3630–3634
40. Burgess, K., and Cook, D. (2000) *Chem. Rev.* **100,** 2047–2060
41. Ludwig, J., and Eckstein, F. (1989) *J. Org. Chem.* **54,** 631–635
42. Yoshikawa, M., Kato, T., and Takenishi, T. (1967) *Tetrahedron Lett.* **50,** 5065–5068
43. Sigel, H., and Sigel, A. (1995) *Metal Ions in Biological Systems: Vanadium and Its Role for Life*, pp. 153–154, Marcel Dekker, Inc., New York
44. Calvo, C. (1967) *Acta Crystallogr.* **23,** 289–295
45. Holloway, C. E., and Melnick, M. (1986) *Rev. Inorg. Chem.* **8,** 287–360
46. Jencks, W. P. (1987) *Catalysis in Chemistry and Enzymology*, pp. 111–112, Dover Publications, New York
47. Tabor, S., and Richardson, C. C. (1987) *Proc. Natl. Acad. Sci. U.S.A.* **84,** 4767–4771
48. Tabor, S., and Richardson, C. C. (1995) *Proc. Natl. Acad. Sci. U.S.A.* **92,** 6339–6343

Downloaded from www.jbc.org at HARVARD UNIVERSITY, on August 13, 2011